The effect of debris-flow sediment grain size distribution on fan forming processes

Haruka Tsunetaka[1], Norifumi Hotta[2], Yuichi Sakai[3], Thad Wasklewicz[4]

[1]Forestry and Forest Products Research Institute, Ibaraki, Japan
5 [2]Graduate School of Agricultural and Life Sciences, The University of Tokyo, Tokyo, Japan
[3]Division of Earth and Planetary Sciences, Graduate School of Science, Kyoto University, Kyoto, Japan
[4]Stantec Inc, Environmental Services, Geohazards and Geomorphology Group, Fort Collins, CO, USA

Correspondence to: Haruka Tsunetaka (tsunetakaharuka@ffpri.affrc.go.jp)

Abstract. Knowledge of the processes driving debris-flow fan evolution are critical in the support of efforts to mitigate
10 related hazards, reduce risk to populations and infrastructure, and reconstruct the history of sediment dynamics in
mountainous areas. Research on debris-flow fan development has focused on topographic controls, debris-flow volume and
rheology, and the sequence of occurrence of debris flows. While these items have explained a great deal about fan formation
and specifically avulsion and runout mechanisms, there is a need to further investigate other properties as they relate to
debris-flow fan formative process. Here, we examined the role of debris-flow grain-size distribution on fan formation. Flume
15 experiments were employed to examine the morphology of debris-flow fans that resulted from flows with mono- or multi-
granular sediment composition with the same average grain size. All other flow characteristics were held constant. The
mono-granular flows formed a symmetric-like fan morphology because there was little avulsion during the formation
process. The multi-granular flows produced fans with an asymmetric morphology. Avulsions occurred on both lateral extents
of the fan during the early stages of fan development and caused the runout direction to shift produce the fan asymmetry.
20 Grain-size distribution was closely related to spatial diversity in fan morphology and stratigraphy.

1 Introduction

Debris-flow fans are substantive sediment sinks persisting greater than 10^2 years in many locations throughout the world
(e.g., Dühnforth et al., 2007; Schürch et al., 2016). An understanding of debris-flow fan sedimentary sequences and the
processes forming individual fan deposits make it possible to reconstruct the climate and sediment dynamics leading to fan
25 development. The findings would be particularly useful in areas where little or no other geomorphological and hydrological
evidence are present, such as arid regions or other planets (e.g., De Haas et al., 2015a, 2019; D'Arcy et al., 2017). Debris-
flow fan forms have been determined to result in great part to autogenic behavior whereby the natural progression is one
where debris flow runout over time involves backfilling of the existing channel on the fan, a loss in channel capacity,
subsequent avulsions, channelization processes, and a repeat of these same process. These cycles are derived from internal
30 forcing and have a direct impact on the fan morphology based on the direction and distance of the runout of subsequent

debris flows (e.g., De Haas et al., 2016, 2018a, b). These cycles highlight the importance of grasping the processes that drive the debris-flow fan formation and to use this information to further inform mitigation solutions to protect the populace and infrastructure located in these vicinities.

Debris-flow fan morphology and stratigraphy are linked to the spatiotemporal patterns of the autogenic fan-forming cycle
35 and are susceptible to differences in the physical parameters of debris flow such as sediment density and grain-size distribution (e.g., Whipple and Dunne, 1992; Pederson et al., 2015). Changes in the physical parameters (e.g., flow rate, duration, and sediment concentration) may give rise to functional changes in debris flows released into the fan apex that may be related to the initial flow state, channel bed slope, and sediment entrainment rate (Egashira et al., 2001; De Haas and Van Woerkom, 2016). These changes may affect debris-flow fan development, and depending on the topographic complexity,
40 could produce varying functional changes in subsequent debris flows. Consequently, both functional and structural changes in debris flows affect the autogenic cycle, which drives each of the debris-flow characteristics that contribute to the patterns of fan formation. By discriminating between the roles of these characteristics, it becomes easier to interpret fan stratigraphy, which will then help us develop more realistic forecasts of debris-flow inundation ranges.

Here, we investigated how the grain-size distribution of debris flows affected the fan-forming processes. We carried out
45 reduced-scale flume tests to compare the debris-flow fan morphology under varying sediment source grain-size distributions. The results from the debris-flow runout and space-time changes in the fan morphology provide insights into how the grain-size distribution affects the fan formative processes.

2 Methods

2.1 Flume test

50 A straight flume (8 m long and 0.1 m wide, with a uniform 15° bed slope, Fig. 1a) connected to a deposition area. A 5-m long section at the lower end of the flume was filled with 0.08 m^3 of sediment particles that were horizontally flattened to the flume bed to achieve analogous erodible bed conditions for all the tests (Fig. 1a). The erodible bed mostly remained constant at 0.2 m deep but sometimes ranged from 0–0.2 m as it was smoothly leveled down the upper and lower end of the erodible bed (Fig. 1a). Sediment particles (~1 mm in diameter) were glued onto the surface of the deposition area to represent the
55 roughness and drew square grid lines (0.2 × 0.2 m) to measure the runout distance and time at which the flow front first arrived at the deposition area (Fig. 1b). A steady flow of clear water was supplied at a rate of 0.003 m^3/s for 60 s from the upper end of the flume. The supplied water generated a granular flow that imitated a single debris-flow surge and then entrained the erodible bed to the deposition area that was connected to the lower end of the flume. The slope of the deposition area decreased from 12° to 3° at a rate of 3° per meter (Fig. 1a, b), and so the fan morphology gradually formed in
60 accordance with the runout and inundation of the released granular flow.

Two types of granular flow, namely mono-granular and multi-granular, were used to determine the impact of grain-size distribution within a debris flow on the fan-forming processes. The experiment maintained similar flow states, but different

grain-size distributions. The grain-size distribution has been shown to affect the properties of the released granular flows, such as the flow depth and velocity (Egashira et al., 2001; Kaitna et al., 2016; Sakai et al., 2019). The experimental

65 conditions were designed to purposely avoid unexpected changes in the flow state caused by very large and small sediment particles by adjusting the mixing ratio of sediment particles used in the flume tests but maintaining the same average grain size (D_{50}) between the mono-granular and multi-granular flows (Fig. 1c and Table 1).

2.2 Measurement and analysis

The flow depths and arrival times of the granular flows were monitored and compared as sediment was released to the

70 deposition area in the various simulations. The flow depth of a generated granular flow cannot be measured in the flume because the thickness of the erodible bed decreases sequentially in response to the sediment entrainment. Therefore, the displacement of the flow surface at three positions in the flume (upper, middle, and lower, Fig. 1a) was measured to account for this shortcoming, using ultrasonic displacement meters (described in Sect. S1 in the Supplement).

Four digital cameras installed above the deposition area (Fig. 1a) observed the fan-formation processes (Tsunetaka et al.,

75 2019). Three of these cameras were automatically synchronized using the external shutter and captured images at 1-s intervals. Using a photogrammetry software, we produced digital elevation models (DEMs) and orthophotos that were geo-referenced by the coordinates of visible (exposed) intersections of the grid lines on the deposition area (i.e., at the intersections of the grid lines that were not concealed by deposited sediment) from respective sets of three synchronized images (Sect. S2). Deposit depths were measured at the intersections of the grid lines when the fans formed, and compared

80 the measurements with the deposition depths extracted from the generated DEM. The measured elevations corresponded to the DEM-extracted elevations, thereby indicating that the DEMs approximated well to the fan morphology (Fig. S1).

The fourth camera recorded a video of the fans as they formed at a frame rate of 60 fps. Paired image sets were extracted from two images at a 1/60-s time resolution from the video. The paired image sets were processed by a particle-image-velocimetry (PIV) algorism to show the vectors of the flow velocity at the surface of the deposition area (Sect. S2). During

85 the inundation of sediment at the deposition area, the SfM-MVS photogrammetry could not measure locations where granular flows descended, which resulted in holes of DEMs due to lacking topographic data (e.g., Fig. 5). The vectors of the flow velocity projected by the PIV analysis could compensate for the holes of DEMs, allowing for the investigation of changes in flow direction caused by avulsions. The used videos were acquired from an almost-vertical direction against the area with a 9° slope. It is worth noting that the shooting depth varied spatially in the angle of view because the camera was

90 not strictly vertical to the whole of the deposition area and spatiotemporal changes in fan morphology, which means that the velocity projected by the PIV analysis was not strictly accurate. The measurements of the flow-velocity vectors were useful to investigate changes in the flow direction that occurred during the fan development, rather than measure flow velocity.

3 Results

3.1 Flow state in the channel

95 Both mono-granular and multi-granular flows descended to the lower position in the flume ~6–7 s upon leaving the arrival point at the upper position (Fig. 2). Given an initial erodible bed thickness of approximately 0.2 m, the peak of the mono-granular flows ranged from ~0.03 to 0.07 m for the test runs, while, apart from run 1, those of the multi-granular flows were around ~0.03 m (Fig. 2). The thickness of the erodible bed decreased monotonically with time, probably because the entrainment rate was the same in all the test runs, irrespective of the grain-size distribution of the granular flows (Fig. 2),

100 which confirms that the released granular flows had reached a steady state. Overall, the results from the flume experiment showed that the difference in the grain-size distribution did not lead to substantial changes in the hydrograph and arrival time of the granular flows.

Exact replication of the dynamic conditions of natural debris flows was not possible in our reduced-scale flume tests, as reported in other similar flume experiments (e.g., De Haas et al., 2015b). The ratios between the flow depth of the front in

105 the channel to the average grain size (i.e., 2.6 mm; Table 1) were between ~10–30, which confirms that the released granular flows that were experimentally modelled as so-called boulder debris flow could be explained as steady laminar flows in terms of their dynamic similarity (Hotta and Miyamoto, 2008).

3.2 Runout of surge front

While the mono- and multi-granular flows in the flume were similar, their runout characteristics differed. The fronts of the

110 mono-granular flows travelled faster and further downstream than those of the multi-granular flows (Fig. 3a, b). Consequently, the velocities of the multi-granular flows from the start to the end of the runout of the front were about ~0.1 m/s less than those of the mono-granular flows (Fig. 3c). Analysis of the grain-size distribution from the center of the multi-granular fans (Figs. S2 and S3) shows that particles were segregated by grain sizes and relatively large particles accumulated at the downstream edge of the flow fronts (Figs. S2f and S3f). The difference in the grain-size distribution of the released

115 flows did not affect the flow in the flume but may have changed the flow velocity and frictional resistance in the deposition area where the grains were segregated by size.

3.3 Formed fan morphology

The flow direction and deposition range differed between the mono-granular and multi-granular flows. In the first 10 s of the flow, both types of granular flow descended in an approximately straight flow direction, but the locations of the lobe-like

120 deposits generated by the flow fronts differed (Figs. 4 and S4). Between 20 and 50 s after the flow was released, the mono-granular flows descended in a straight line through the zone with a 9°–12° slope without substantial avulsion, but then showed some avulsion in the zone on a 6° slope (Figs. 5–8 and S5–S8). The multi-granular flow, 20 s after being released, avulsed obviously as the deposition around the downstream edge of the fan had impeded the descent of the flow that

followed (Figs. 5 and S5). More than ~30 s after the multi-granular flows were released (Figs. 6–8 and S6–S8), the flow
125 directions migrated to the left or right side of the deposition area near a slope angle of 9°.

The final deposition ranges of the mono-granular fans were similar (Figs. 9a–d and S9a–d), whereas the multi-granular flows
formed bilaterally asymmetric deposits that varied between test runs (Figs. 9e–h and S9e–h). For example, the fans generated
by the multi-granular test runs 2 and 3 were elongated to the left bank side, while those of runs 1 and 4 were elongated to the
right bank side (Figs. 9e–h and S9e–h).

130 The mono-granular flows had similar profiles and bilaterally symmetrical fan morphologies (Fig. 10a, d, g). Similarly, the
multi-granular fans had similar longitudinal profiles, irrespective of the elongated direction (Fig. 10b). However, the multi-
granular flows were less deep than the mono-granular runs in the area 2 m downstream from the flume outlet (Fig. 10c).
Although the peaks of the deposition depth of the longitudinal profiles were similar between the multi-granular and mono-
granular flows (Fig. 10a–c), the flows were laterally wider and larger 1 m downstream from the flume outlet (Figs. 10d–f).

135 There were noticeable differences in the deposition depths of the mono-granular and multi-granular flows at the cross section
2.2 m downstream from the flume outlet (Fig. 10g–i). The deposition depths of the multi-granular flows varied by more than
0.03 m, depending on the direction of the elongated fan (Fig. 10i). The fan widths of the multi-granular flows were notably
larger again at 2.2 m (Fig. 10g–i). A larger fan width is an expected consequence of the avulsion observation and PIV
support information from the multi-granular flow modelled scenarios.

140 4 Discussion

The fan-forming processes and the sediment deposition and stratigraphy changed in response to changes in grain-size
distribution of the released granular flows, while holding all other conditions constant. Some equations that describe debris
flows assume that multi-granular debris flows can be approximated to mono-granular debris flows with the same average
grain-size (e.g., Egashira et al., 1997; Takahashi, 2007). However, the mono-granular and multi-granular flows with the
145 same average grain-size produced fans with different morphologies, and the fans that resulted from the multi-granular flows
also varied between the test runs (Figs. 9 and 10), which indicates that existing models that assume a mono-granular
approximation may provide ambiguous simulations of the debris-flow deposition and inundation ranges.

The fronts of the multi-granular flows were comprised of relatively large sediment particles (Figs. S2 and S3), reflecting
grain-size segregation often discussed in the literature (e.g., Johnson et al., 2012) and evidenced in the field. These large
150 particles may increase the flow frictional resistance (e.g., De Haas et al., 2015b; Hürlimann et al., 2015), which may help
explain why the runout distance and velocity of the released multi-granular flow fronts were shorter and lower than those of
the mono-granular flows, respectively (Fig. 3). The flow rates and arrival times of the mono- and multi-granular runs were
almost the same in the flume (Fig. 2). This finding suggests that the thick and short lobe-like deposits of the multi-granular
flows reflected the shorter runout distances (Figs. 4 and 10c), which may in turn have triggered the pronounced avulsion
155 further upstream of the deposition area that did not form for the mono-granular flows (Figs. 5–8 and S5–S8).

The thick and short deposits with surfaces comprised of large particles identified in the early stage of the fan-forming processes might facilitate the dispersion and seepage of the pore fluid through the fan because of its high permeability, and lead to unsaturated conditions at the fan surface. Other researchers, through field measurements and flume experiments, have shown that deposition of debris flows may be triggered when the surfaces of channel beds are highly permeable and

160   unsaturated (e.g., Major and Iverson, 1999; Staley et al., 2011; Tsunetaka et al., 2019). As there was little difference between the runout characteristics of the multi-granular test runs (Figs. 3b and 4e–h), the variations in the fan morphology may reflect spatial and temporal variations in the degree of saturation throughout the fan. If this is the case, even processes that drive mono-granular fan formation may vary among test runs, particularly when mono-granular flows comprise large particles that can facilitate the dispersion and seepage of pore-fluid in a formed fan.

165   This examination of the grain-size distribution of debris flows shows that fan-forming processes are complex and reflect the interactions between their functional and structural characteristics. The differences in the experimental fan morphometries highlight how varying orders of grain-size distribution strongly impact debris-flow fan development and produced varying stratigraphic layers. The findings also considered the moisture regime of the experimental fan evolution, which improves the accuracy and reliability of forecasts of the deposition and inundation ranges of debris flows around channel outlets.

170

5 Conclusions

While it is accepted that the morphology of debris-flow fan depends on the characteristics of the debris flow that is released to the fan apex (e.g., flow stage and sediment concentration), there is still considerable debate about how changes in these characteristics impact fan-forming processes. In this study, changes in fan morphology were investigated, with a particular

175   focus on the grain-size distribution of the released debris flow. We carried out reduced-scale flume experiments to model the morphology of debris-flow fans that resulted from flows that were mono- or multi-granular with the same average grain size, but with all other flow characteristics the same. The mono-granular flows formed a symmetric-like fan morphology because there was little avulsion during the formation process. The multi-granular flows produced fans with asymmetric morphology, and had avulsions on both sides during the early stages of the inundation, which caused the runout direction to shift as the

180   topography evolved. Our results show that the grain-size distribution was closely related to spatial diversity in fan morphology and stratigraphy.

Data availability

The data used in this study are freely available from the corresponding author upon request.

Author contribution

185 HT designed the study, carried out flume tests and all analyses, and wrote the paper. NH and YS supported flume tests, provided input for the result interpretations, and reviewed and edited the paper. TW was involved in conceptualizing the study, shaping the methodology and discussion, and writing the paper.

Acknowledgement

The authors are grateful to the staff of CTI Engineering Co., Ltd. for their assistance in the flume test.

190 **Conflicts of Interest**

The authors declare they have no conflict of interest.

Funding

The research was supported by JSPS KAKENHI (grant numbers 18J01961 and 19KK0392).

References

195 D'Arcy, M., Roda-Boluda, D.C., and Whittaker, A.C., 2017, Glacial-interglacial climate changes recorded by debris flow fan deposits, Owens Valley California: Quaternary Science Reviews, v. 169, p. 288–311.

De Haas, T., Hauber, E., Conway, S.J., van Steijn, H., Johnsson, A., and Kleinhans, M.G., 2015a, Earth-like aqueous debris-flow activity on Mars at high orbital obliquity in the last million years: Nature Communications, v. 6, 7543.

De Haas, T., Braat, L., Leuven, J.R., Lokhorst, I.R., and Kleinhans, M.G., 2015b, Effects of debris flow composition on

200 runout, depositional mechanisms, and deposit morphology in laboratory experiments: Journal of Geophysical Research: Earth Surface, v. 120, p. 1949–1972.

De Haas, T., and Van Woerkom, T., 2016, Bed scour by debris flows: experimental investigation of effects of debris-flow composition: Earth Surface Processes and Landforms, v. 41, p. 1951–1966. DOI: 10.1002/esp.3963.

De Haas, T., Berg, W., Braat, L., and Kleinhans, M.G., 2016, Autogenic avulsion, channelization and backfilling dynamics

205 of debris-flow fans: Sedimentology, v. 63, p. 1596–1619.

De Haas, T., Densmore, A.L., Stoffel, M., Suwa. H., Imaizumi, F., Ballesteros-Cánovas, J.A., and Wasklewicz, T., 2018a, Avulsions and the spatio-temporal evolution of debris-flow fans: Earth-Science Reviews, v. 177, p. 53–75. DOI: 10.1016/j.earscirev.2017.11.007.

De Haas, T., Kruijt, A., and Densmore, A.L., 2018b, Effects of debris-flow magnitude-frequency distribution on avulsions

210   and fan development: Earth Surface Processes and Landforms, v. 43, p. 2779–2793. DOI: 10.1002/esp.4432.

De Haas, T., Densmore, A.L., den Hond, T., and Cox, N.J., 2019, Fan-surface evidence for debris-flow avulsion controls and probabilities, Saline Valley, California: Journal of Geophysical Research: Earth Surface, v. 124, p. 1118–1138. DOI: 10.1029/2018JF004815.

Dühnforth, M., Densmore, A.L., Ivy-Ochs, S., Allen, P.A., and Kubik, P.W., 2007, Timing and patterns of debris flow

215   deposition on Shepherd and Symmes Creek fans, Owens Valley, California, deduced from cosmogenic 10Be: Journal of Geophysical Research: Earth Surface, v. 112, F03S15. DOI: 10.1029/2006JF000562.

Egashira, S., Miyamoto, K., and Itoh, T., 1997, Constitutive equations of debris flow and their applicability. In Debris Flow Hazards Mitigation/Mechanics, Prediction, and Assessment: Proceedings of 1st International Conference, California, USA; 340–349.

220   Egashira, S., Honda, N., and Itoh, T., 2001, Experimental study on the entrainment of bed material into debris flow: Physics and Chemistry of the Earth, Part C: Hydrology, Ocean and Atmosphere, v. 26, p. 645–650.

Hotta, N., and Miyamoto, K., 2008, Phase classification of laboratory debris flows over a rigid bed based on the relative flow depth and friction coefficients: International Journal of Erosion Control Engineering, v. 1, p. 54–61.

Hürlimann, M., McArdell, B.W., and Rickli, C., 2015, Field and laboratory analysis of the runout characteristics of hillslope

225   debris flows in Switzerland: Geomorphology, v. 232, p. 20–32.

Johnson, C.G., Kokelaar, B.P., Iverson, R.M., Logan, M., Lahusen, R.G., and Gray, J.M.N.T., 2012, Grain-size segregation and levee formation in geophysical mass flows: Journal of Geophysical Research: Earth Surface, v. 117, p. 1–23.

Kaitna, R., Palucis, M.C., Yohannes, B., Hill, K.M., and Dietrich, W.E., 2016, Effects of coarse grain size distribution and fine particle content on pore fluid pressure and shear behavior in experimental debris flows: Journal of Geophysical

230   Research: Earth Surface, v. 121, p. 415–441.

Major, J.J., and Iverson, R.M., 1999, Debris-flow deposition: Effects of pore-fluid pressure and friction concentrated at flow margins: Geological Society of America Bulletin, v. 111, p. 1424–1434.

Pederson, C.A., Santi, P.M., and Pyles, D.R., 2015, Relating the compensational stacking of debris-flow fans to characteristics of their underlying stratigraphy: Implications for geologic hazard assessment and mitigation: Geomorphology,

235   v. 248, p. 47–56.

Sakai, Y., Hotta, N., Kaneko, T., and Iwata, T., 2019, Effects of grain-size composition on flow resistance of debris flows: behavior of fine sediment: Journal of Hydraulic Engineering, v. 145, 06019004.

Staley, D.M., Wasklewicz, T.A., Coe, J.A., Kean, J.W., McCoy, S.W., and Tucker, G.E., 2011, Observations of debris flows at Chalk Cliffs, Colorado, USA: Part 2, changes in surface morphometry from terrestrial laser scanning in the summer of

240   2009. In Debris Flow Hazards Mitigation/Mechanics, Prediction, and Assessment: Proceedings of 5th International Conference, Padua, Italy; 759–768.

Schürch, P., Densmore, A.L., Ivy-Ochs, S., Rosser, N.J., Kober, F., Schlunegger, F., McArdell, B.W., and Alfimov, V., 2016, Quantitative reconstruction of late Holocene surface evolution on an alpine debris-flow fan: Geomorphology, v. 275, p. 46–57.

245   Takahashi T., eds., 2007, Debris flow: Mechanics, Prediction and Countermeasures: Taylor & Francis, Leiden, 448 p.

Tsunetaka, H., Hotta, N., Sakai, Y., Nishiguchi, Y., and Hina, J., 2019, Experimental examination for influence of debris-flow hydrograph on development processes of debris-flow fan. In Debris Flow Hazards Mitigation/Mechanics, Prediction, and Assessment: Proceedings of 7th International Conference, Colorado, USA; 443–450.

Whipple, K.X., and Dunne, T., 1992, The influence of debris-flow rheology on fan morphology, Owens Valley, California:

250   Geological Society of America Bulletin, v. 104, p. 887–900.

Table 1: Sediment particles and mixing ratio.

Range of grain size (mm)	Average grain size (mm)	Mixing ratio of mono-granular (%)	Mixing ratio of multi-granular (%)
0.6–0.8	0.7	0	10
0.8–1.36	1.1	0	12.5
1.36–2.02	1.7	0	15
2.02–3.24	2.6	100	25
3.24–4.57	3.9	0	15
4.57–5.85	5.2	0	12.5
5.85–7.5	6.7	0	10

255

260
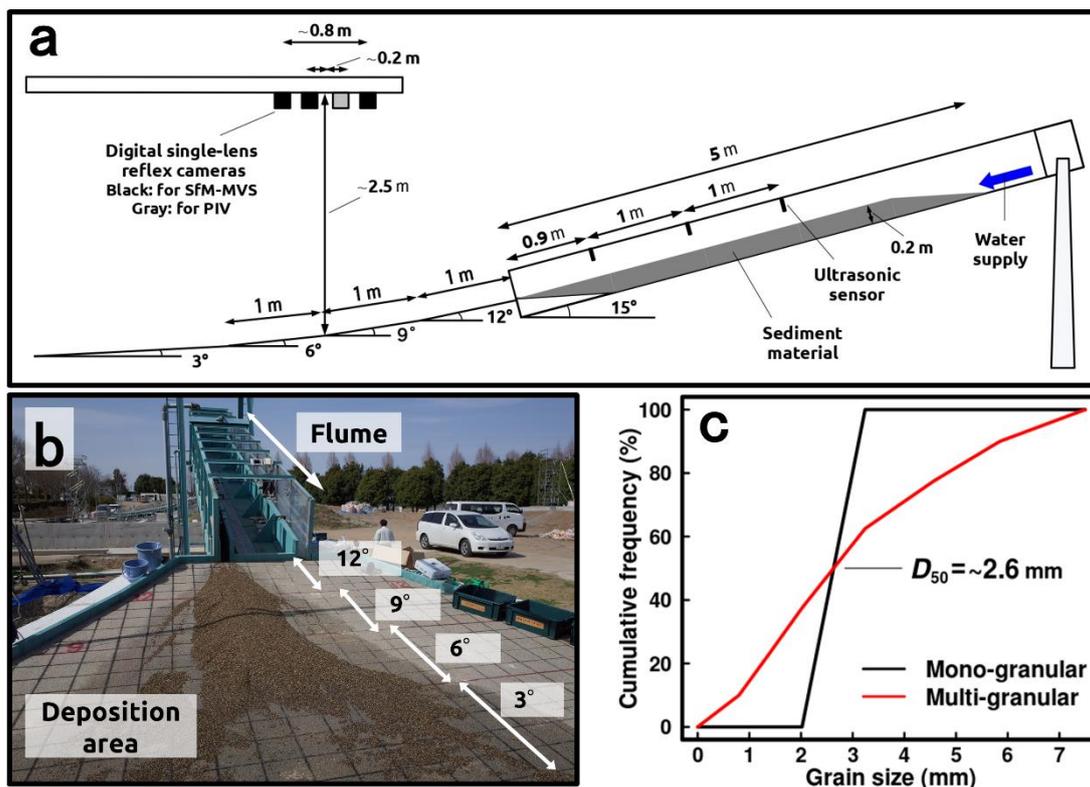
Figure 1: Test flume setup. (a) Dimensions of the test flume and equipment. (b) View of the channel and the deposition area. (c) Grain-size distribution of the sediment materials used in the experiments. Figure modified from Tsunetaka et al. (2019).

Earth **Surface**
Dynamics
Discussions
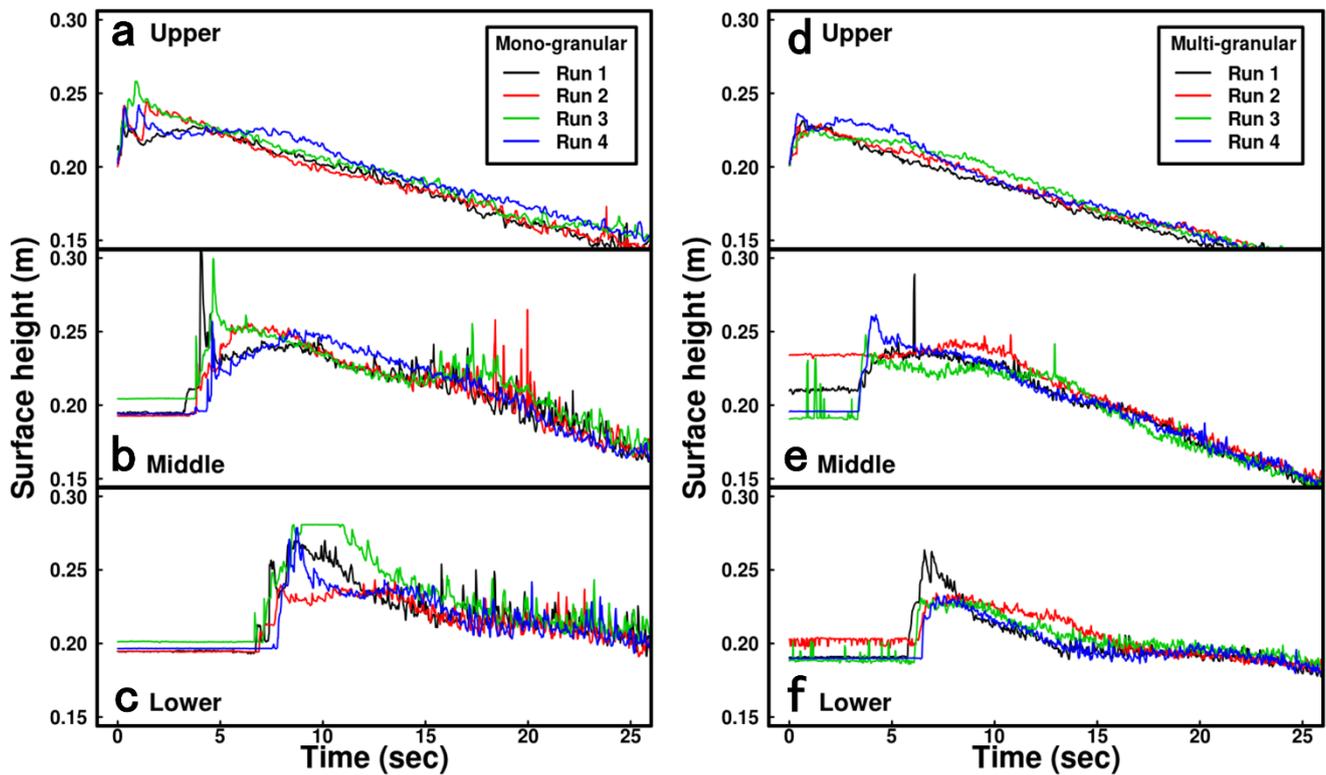
Figure 2: Changes in the debris-flow surfaces. (a–c): mono-granular flows. (d–f): multi-granular flows. The time (x-axis) was set to assume that the flow front arrived at the upper point at zero. Any change in the initial thickness of the bed surface (e.g., Fig. 2e) due to local undulation was probably cancelled out by the debris-flow descent (see Sect. S1 in the Supplement).
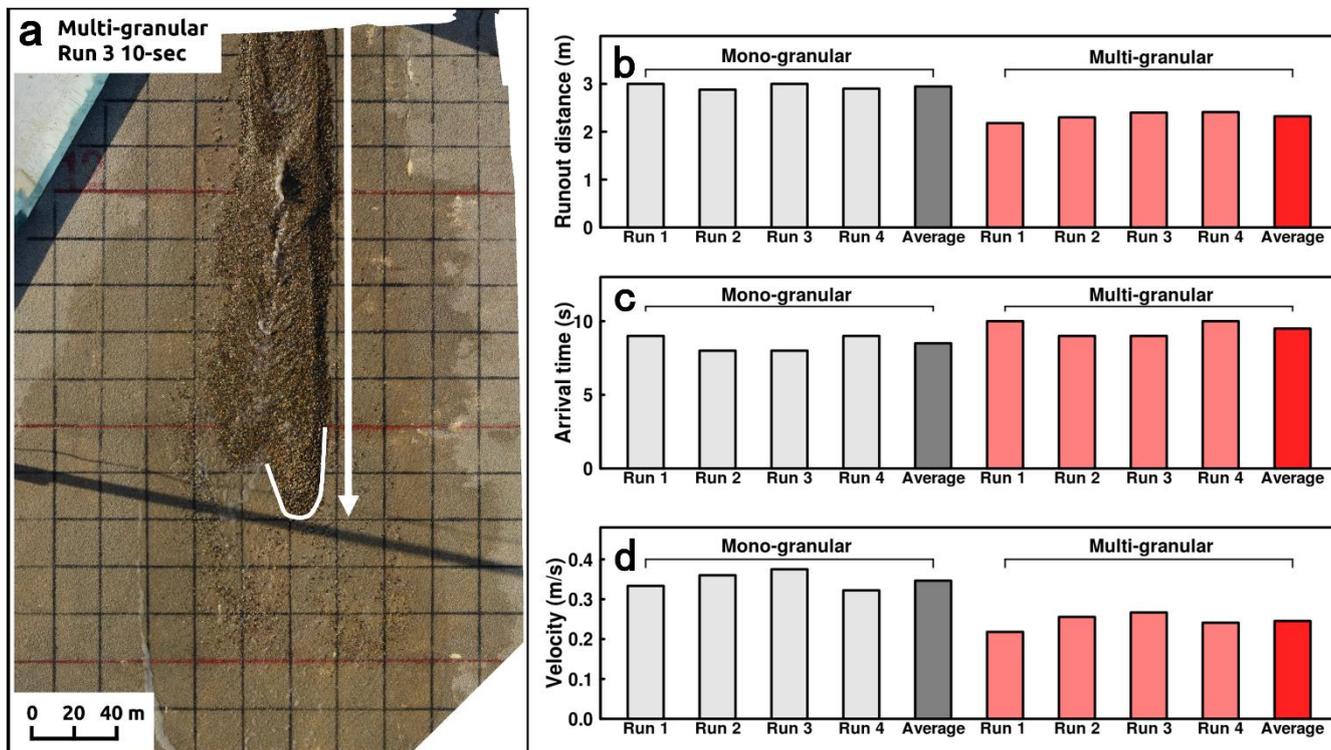
Figure 3: Runout characteristics of the flow fronts at the deposition area. (a) orthophoto for a multi-granular flow (run 3) approximately
275 10 s after the start of the runout. The white arrow and line indicate the runout distance and the location of the front, respectively. (b)
comparison of the total runout distance of the flow fronts. (c) comparison of the arrival time of the flow fronts at the deposition area. (d)
comparison of the velocity (the ratio of the runout distance to the arrival time).
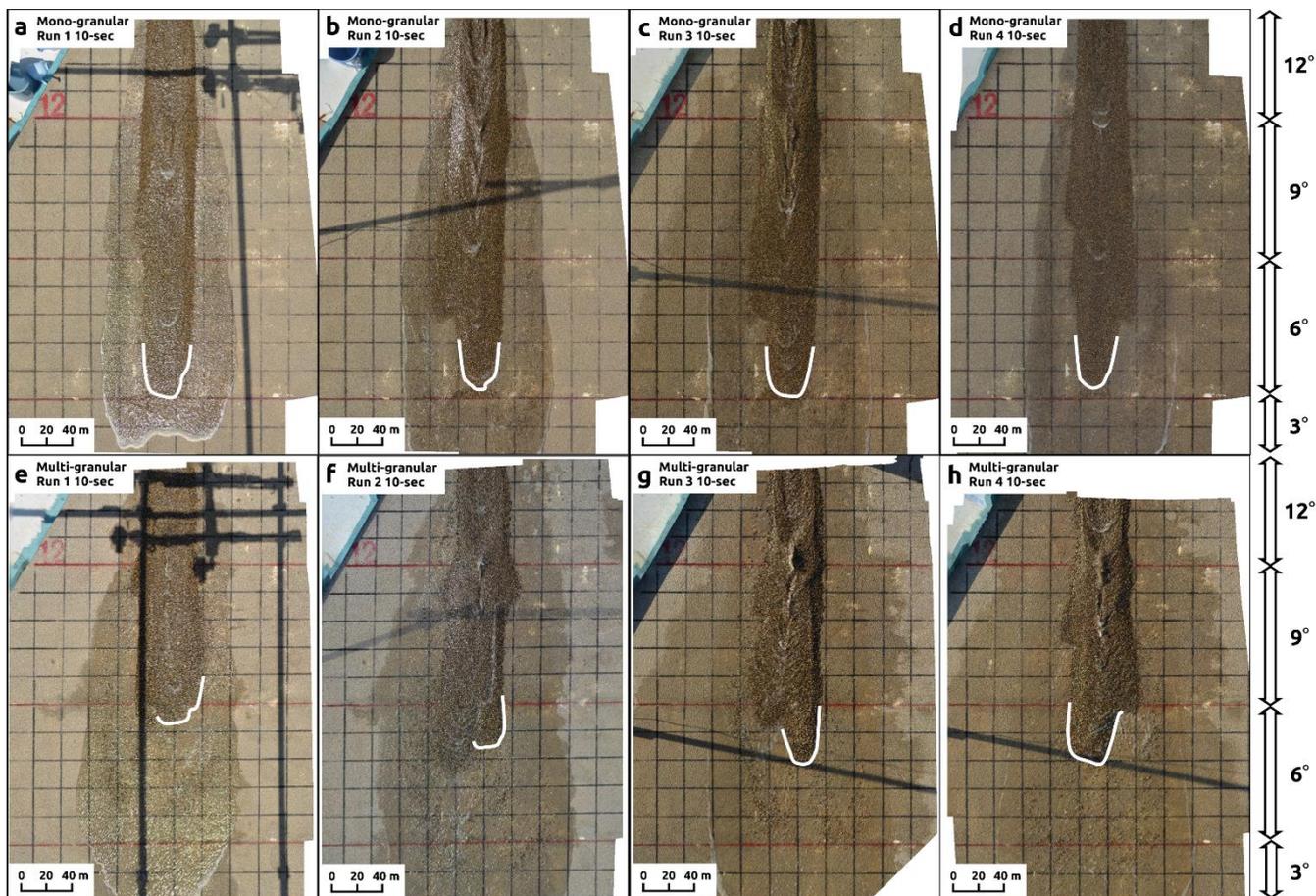
Figure 4: Orthophoto 10 seconds after the start of the runout. (a–d) Mono-granular flows. (e–h) Multi-granular flows. The white line indicates the flow front.
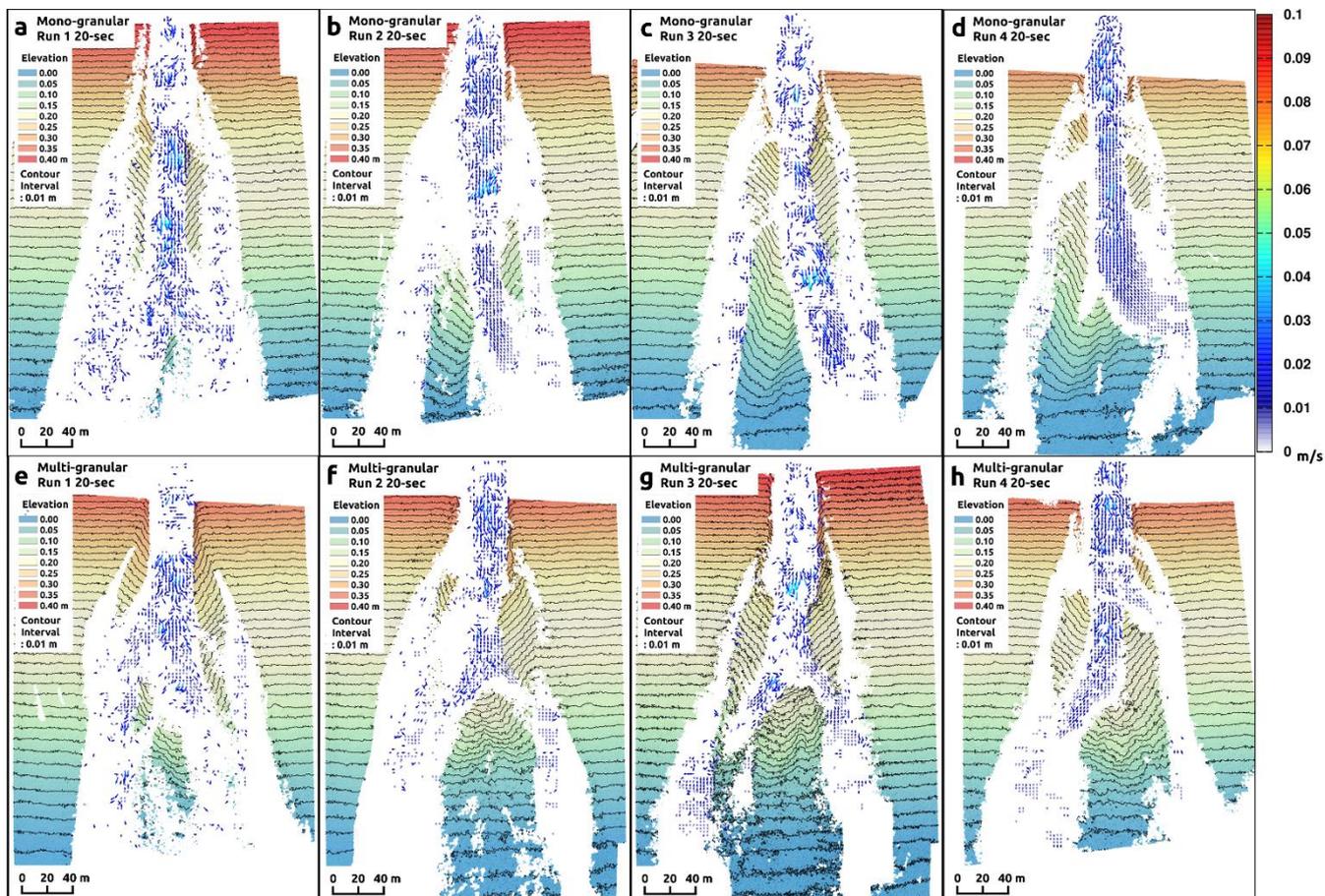
Figure 5: Fan formation and distribution of the flow vectors 20 seconds after the start of the runout. (a–d) Mono-granular flows. (e–h) Multi-granular flows. The elevation is depicted assuming that the area with a 3° slope (i.e., the area further downstream from where the slope angle changed from 3° to 6° slope) has an elevation of zero.
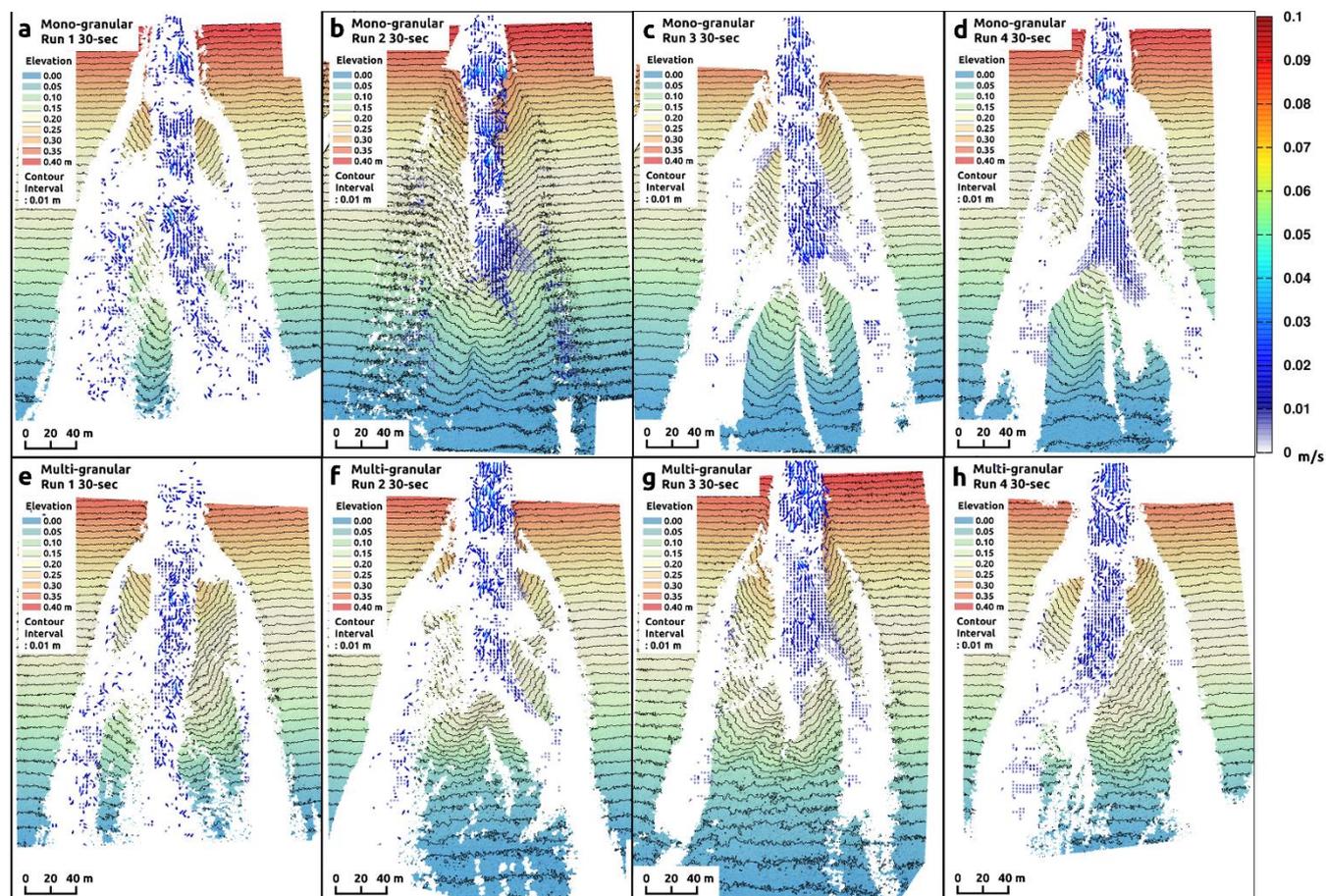
Figure 6: Fan formation and distribution of the flow vectors 30 seconds after the start of the runout. (a–d) Mono-granular flows. (e–h) Multi-granular flows. The elevation is depicted assuming that the area with a 3° slope (i.e., the area further downstream from the point where the slope changed from 3° to 6°) has an elevation of zero.
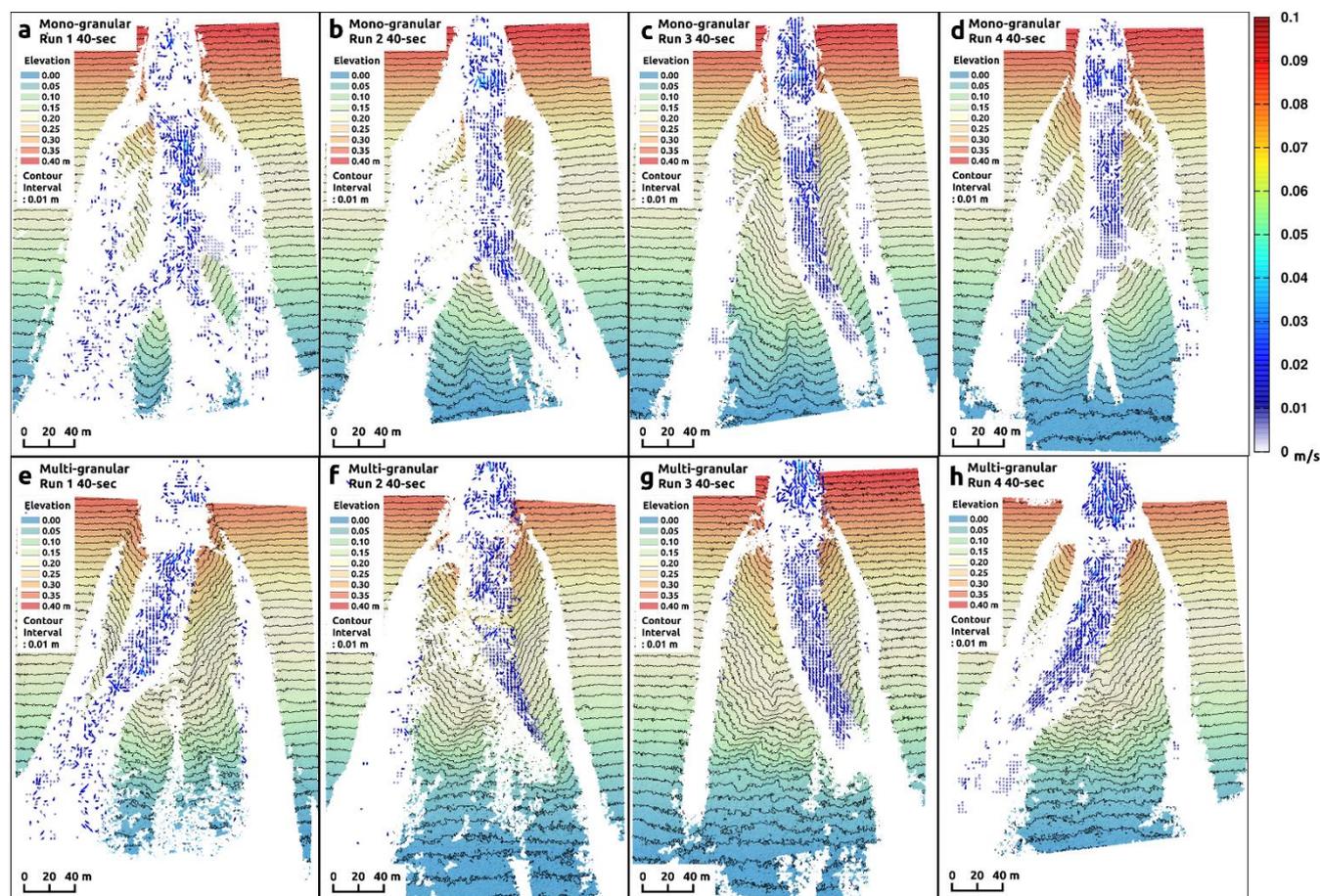
Figure 7: Fan formation and distribution of the flow vectors 40 seconds after the start of the runout. (a–d) Mono-granular flows. (e–h) Multi-granular flows. The elevation is depicted assuming that the area with a 3° slope (i.e., the area further downstream from the point where the slope changed from 3° to 6°) has an elevation of zero.
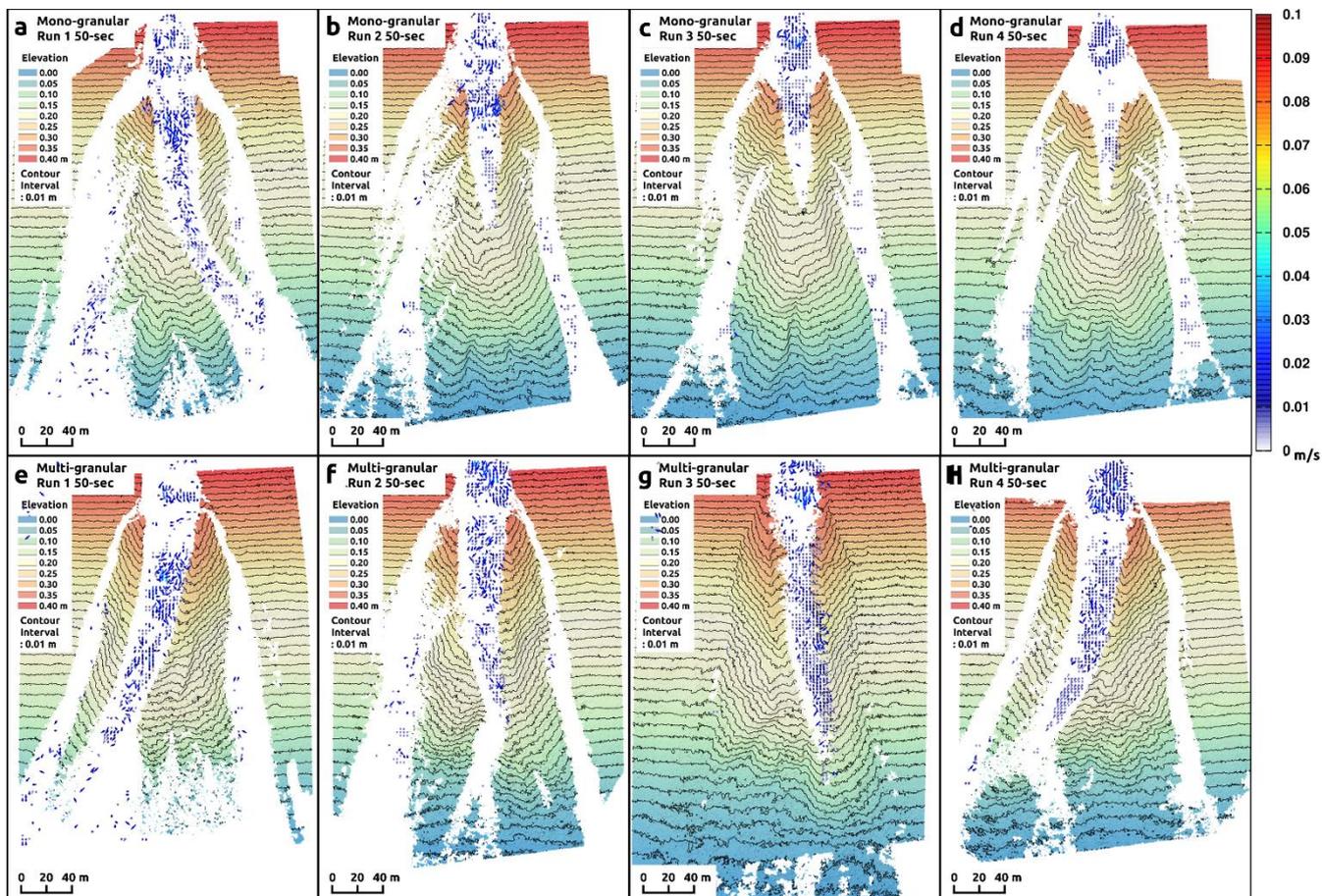
Figure 8: Fan formation and distribution of the flow vectors 50 seconds after the start of the runout. (a–d) Mono-granular flows. (e–h)
Multi-granular flows. The elevation is depicted assuming that the area with a 3° slope (i.e., the area further downstream from the point
where the slope changed from 3° to 6°) has an elevation of zero.
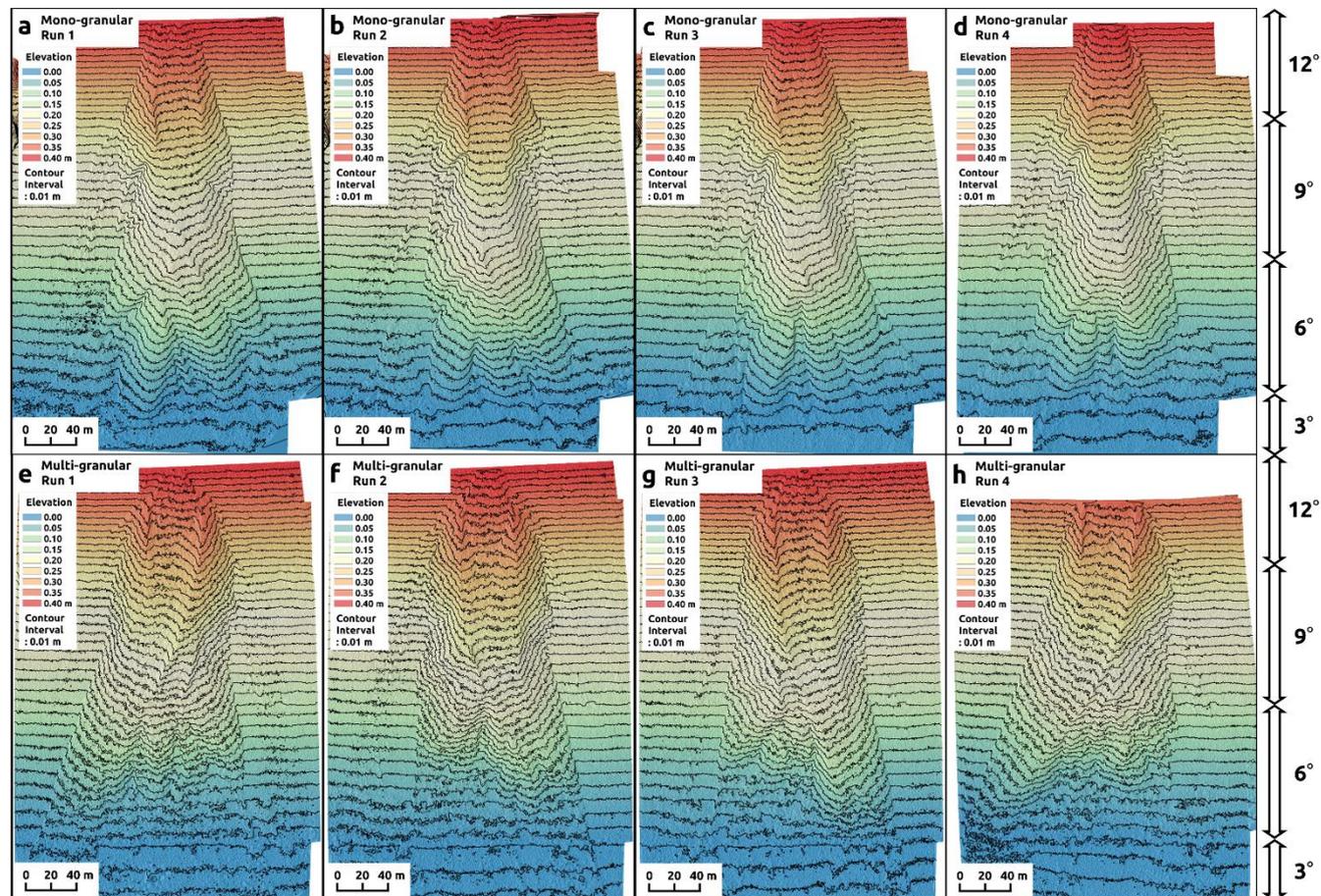
Figure 9: Final topographies of the debris-flow fans. (a–d) mono-granular flows. (e–h) multi-granular flows. The elevation is depicted assuming that the area with a 3° slope (i.e., the area further downstream from the point where the slope changed from 3° to 6°) has an elevation of zero.
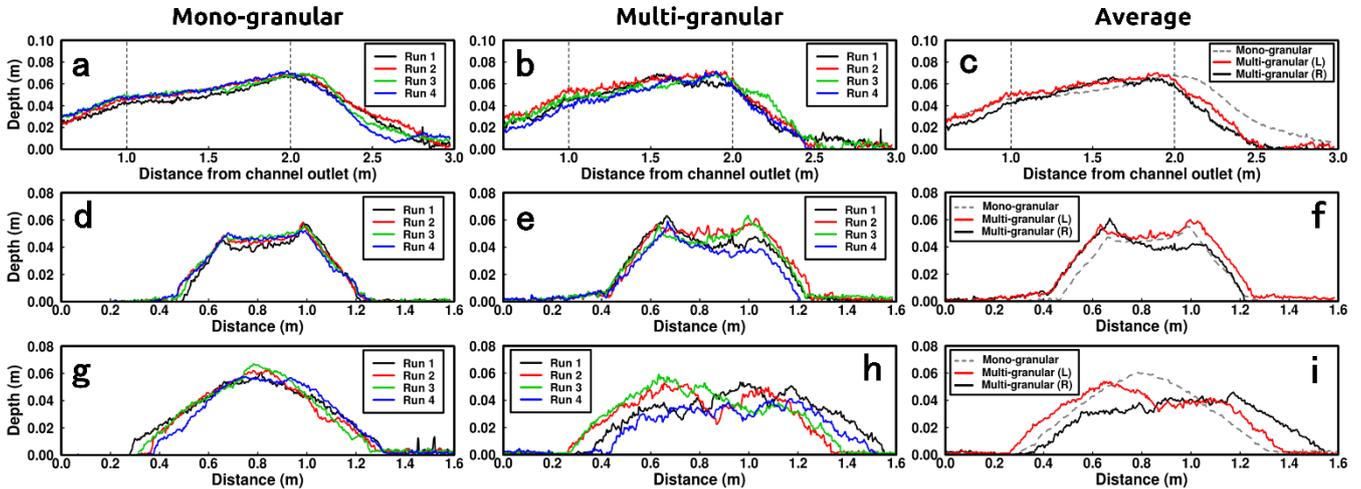
Figure 10: Profiles for the final fans. The left, center, and right panels indicate mono-granular flows, multi-granular flows, and averages, respectively. (a–c) Longitudinal profiles at the center of the fan. Vertical broken lines indicate the boundary of the bed slope (i.e., the change points from 12° to 9° and from 9° to 6°). (d–f) cross section (transverse profile) located 1 m downstream from the flume outlet. (g–i) cross section (transverse profile) located 2.2 m downstream from the flume outlet. In panels d–i, the x-axis indicates the distance from the left-bank side end of the cross sections (the fan was centered at around 0.8 m). In panels c, f, and i, the broken gray line indicates the average value of all the mono-granular flows. The red and black lines indicate the average values of the flows that produced fans that were elongated on the left bank side (i.e., runs 2 and 3) and on the right bank side (runs 1 and 4), respectively.